Shock Wave Induced Decomposition of RDX: Time-Resolved Spectroscopy

James E. Patterson, Zbigniew A. Dreger,* Maosheng Miao, and Yogendra M. Gupta

Institute for Shock Physics and Department of Physics, Washington State University, Pullman, Washington 99164-2816

Received: January 28, 2008; Revised Manuscript Received: April 21, 2008

Time-resolved optical spectroscopy was used to examine chemical decomposition of RDX crystals shocked along the [111] orientation to peak stresses between 7 and 20 GPa. Shock-induced emission, produced by decomposition intermediates, was observed over a broad spectral range from 350 to 850 nm. A threshold in the emission response of RDX was found at about 10 GPa peak stress. Below this threshold, the emission spectrum remained unchanged during shock compression. Above 10 GPa, the emission spectrum changed with a long wavelength component dominating the spectrum. The long wavelength emission is attributed to the formation of NO_2 radicals. Above the 10 GPa threshold, the spectrally integrated intensity increased significantly, suggesting the acceleration of chemical decomposition. This acceleration is attributed to bimolecular reactions between unreacted RDX and free radicals. These results provide a significant experimental foundation for further development of a decomposition mechanism for shocked RDX (following paper in this issue).

I. Introduction

Shockwave initiation of high explosives (HE) is a complex process, and the fundamental chemical reactions that take place during decomposition are not easily identified. To improve current understanding of shock induced HE decomposition, we examined the response of RDX (hexahydro-1,3,5-trinitro-*s*-triazine) single crystals to well-defined planar shock waves. Time-resolved optical spectroscopy was used to investigate the chemical decomposition of shocked RDX in real time. Quantum chemistry calculations complemented the shock wave experiments, as discussed in our companion paper.[1]

RDX is one of a class of energetic molecular crystals known as secondary explosives. Generally stable at ambient conditions, these materials decompose explosively with proper stimulus and are of considerable practical interest. However, sensitivity to initiation raises concerns regarding safety and handling and a better understanding of shock-induced decomposition is needed to optimally address performance and safety issues.

Our laboratory has had a sustained interest in the molecular level response of shocked energetic materials. Time-resolved electronic and vibrational spectroscopies and ab initio calculations led to a proposed decomposition mechanism for shocked Pentaerythritol tetranitrate (PETN).[2–5] A comprehensive research approach is now being applied to RDX. Previously, we observed a shock induced phase transition in unreacted RDX single crystals at stresses of about 4 GPa.[6] Static high pressure experiments have indicated that intermolecular interactions change in the high pressure phase.[7] In this work, we extended our RDX studies to higher shock stresses to investigate shock-induced decomposition.

Many studies, employing a variety of stimuli, have examined the chemical mechanisms of RDX decomposition. Shock wave studies have been quite limited;[8–13] although experiments showed luminescence from RDX crystals around 10 GPa, no chemically significant information was extracted.[9,12,13] Three main mechanisms have been proposed for RDX decomposition:[14] concerted triple ring fission to produce three methylenenitramine (CH_2NNO_2) fragments, homolytic N−N bond scission, and unimolecular HONO elimination. Experimental evidence exists for all three mechanisms. Because the experiments were performed under a variety of stimuli and conditions, the relevance of these results to shock-induced decomposition of RDX crystals is unclear.

The triple ring scission mechanism was observed in gas phase experiments,[15–17] but not in the condensed phase decomposition of RDX.[18] The activation energy for this channel is significantly higher than for the other two mechanisms.[14,19] In addition, the activation volume for this process is considerably greater than for the other two processes.[20] Thus, triple ring fission, though a viable decomposition channel for gas phase RDX, is likely not the first step in the decomposition of crystalline RDX.

Unimolecular N−N bond homolysis has often been suggested as the first decomposition step for RDX[8,18,21–23] and NO_2 has been identified as a reaction product.[8,18,24] In these experiments, however, the breaking of the N−N bond was not observed in real time. Multiple computational studies also support the concept of homolysis being the first decomposition step.[19,21,23,25,26]

Thermal decomposition experiments of RDX in solution found that the activation volume was not consistent with homolysis as the first step. Instead, the results support the HONO elimination mechanism.[27,28] Further, these experiments were carried out to pressures of only 1.1 GPa. This is significantly below shock initiation conditions, raising questions about the applicability of this mechanism to solid-state decomposition under shock loading. However, calculations of the HONO elimination pathway for a single RDX molecule indicate that it is energetically competitive with N−N homolysis.[14,26]

Other mechanisms have also been put forward. A series of papers on the thermal decomposition of solid RDX identified a deuterium kinetic isotope effect (DKIE), suggesting that C−H bond cleavage may be a rate limiting step.[29–33] This observation may be consistent with N−N homolysis as the initial step, followed by ring decomposition or bimolecular reactions that abstract hydrogen.[23] A very different mechanism for decomposi-

* Corresponding author. E-mail: dreger@wsu.edu.

10.1021/jp800827b CCC: $40.75
Published on Web 07/22/2008

tion is suggested by ultrafast photodecomposition experiments where NO was observed as an early reaction product rather than NO_2.[34]

The variety of reported reaction products and decomposition pathways illustrates the need for real-time measurements of shock induced RDX decomposition. In this paper, we report on the application of time-resolved spectroscopy to investigate the response of RDX single crystals to shock wave compression. Continuum calculations provided estimates of the stress and temperature states of the unreacted sample.[35] In a companion paper, we apply quantum chemistry calculations to better interpret our data in terms of specific chemical reactions.[1] This comprehensive approach provides a more complete picture of shocked RDX decomposition.

We have focused on the following questions. First, what is the threshold for the decomposition of shocked RDX? Second, what is the chemical mechanism for the shock-induced decomposition of RDX? Finally, are there temporal characteristics to the decomposition? The remainder of this paper is organized as follows. The next section describes experimental techniques. Experimental results and discussion are presented in section III. Section IV contains concluding remarks. Results of the quantum chemical calculations and the comprehensive decomposition scheme are presented in the companion paper.[1]

II. Experimental Approach

RDX single crystals were grown at the Los Alamos National Laboratory (LANL) from stock produced by the Woolwich (HMX-free) process with additional purification before crystallization. The crystals were oriented along the [111] crystallographic direction, cut, and provided to us by Dr. Daniel E. Hooks of LANL. Typical lateral dimensions of the prepared samples were 7−8 mm. Each crystal was ground to a thickness of ~400 μm and polished to an optical finish with aluminum oxide lapping sheets. The polished RDX crystal was then sandwiched between two optical windows with a thin capillary film of liquid glycerol (spectroscopic grade, Aldrich Chemical) between the crystal and the windows. This liquid layer is only a few micrometers thick and ensures good mechanical contact in the sample cell. In a separate set of control experiments, we verified that glycerol remains optically transparent and chemically inert under the loading conditions of interest. The front window was [100] oriented LiF and the back window was *a*-axis sapphire, except for the highest stress experiment which had a LiF back window. The thicknesses of the front and back windows were 3.05 and 9.5 mm, respectively. Details regarding our experiments are summarized in Table 1.

The overall experimental approach is similar to that used in the PETN work,[3] and a schematic view of the impact experiment is shown in Figure 1. Light emitted from shocked RDX was collected as illustrated in Figure 1. The sample assembly was impacted with a 12.7 mm thick sapphire crystal mounted on a projectile to produce a planar shock wave. A single stage light-gas gun launched the projectile. In the 20 GPa emission experiment, the impactor was a 3.3 mm thick disk of OFHC Cu launched using a powder gun. Upon impact, a shock wave propagated through the front LiF window and into the RDX crystal. The sample was compressed under stepwise loading due to the differing shock impedances of RDX and the window materials. The final stress state of the RDX crystal can be accurately determined because it depends only on the impact velocity, the impactor and the shock wave response of the windows. All of these parameters are well-known. Stress histories in the RDX crystal were calculated using a 1-dimensional wave propagation code[36] and a preliminary, but reasonable, RDX material model.[35] Peak stresses ranged between 7 and 20 GPa.

TABLE 1: Summary of Shock Experiments

no.	experiment type	crystal orientation	sample thickness (μm)	projectile velocity (km/s)	peak stress (GPa)
1	Raman	[111]	400	0.567	10.0
2	Raman	[111]	385	0.873	16.0
3	emission[a]	[111]	395	0.560	9.9
4	emission	[111]	405	0.555	9.8
5	emission	[111]	390	0.720	13.0
6	emission[b]	[111]	390	1.606	20.0
7	emission	[111]	400	0.406	7.0
8	emission	[111]	330	0.646	11.5
9	transmission	[111]	410	0.562	9.9
10	transmission	[111]	400	0.402	6.9
11	transmission	[111]	390	0.721	13.0

[a] First emission experiment was performed with different streak camera system than all others. [b] OFHC Cu impactor and LiF back window. Experiment performed on powder gun.

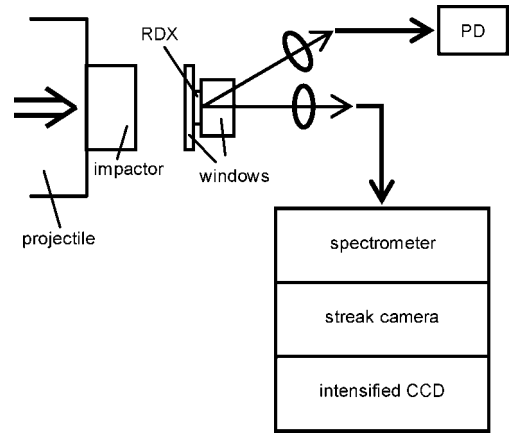

Figure 1. Schematic diagram of time-resolved emission experiment. Emitted light is collected with optical fibers and detected by a diagnostic photodiode (PD) and the spectrometer/streak camera/intensified CCD detection system.

Three time-resolved spectroscopic techniques were employed in this investigation: emission, transmission, and Raman spectroscopy. For emission experiments,[3] the detection system indicated in Figure 1 was used. Light produced by the shocked crystal was collected and transmitted to the detection system using optical fibers. A tunable spectrograph with a low dispersion (150 groove/mm) grating allowed for spectral coverage from 300 to 850 nm. The spectrally dispersed light was coupled to the streak camera/CCD detection system to produce a time dependent emission spectrum. Spectra at particular times were generated by averaging over an appropriate number of tracks on the time axis. The spectral resolution of this system was ~6 nm. The time resolution was ~40 ns, determined by the spot size on the detector. Additional optical fibers coupled the target assembly to a diagnostic photodiode. We characterized the detection system for wavelength dependent instrument response using a tungsten-filament quartz halogen lamp as a calibrated intensity source. By comparing the recorded spectrum of this lamp with the tabulated spectral intensities, we generated an instrument correction function that was applied to all emission data.[3]

The method for performing single pass transmission measurements under shock compression is well established.[37,38] A pulsed Xe flash lamp was the light source. Mirrors mounted on the

projectile cap collimated and directed the lamp output through the sample. Transmitted light was collected by an optical fiber and sent to a spectrometer-streak camera-CCD detection system. Both reference and ambient spectra were collected prior to the shock experiment, allowing the transmission data to be converted to extinction data.[39]

Because of concerns that some extinction could be due to scattering, additional lens units collected light off the main optic axis. Only two sources of light contribute to the signal detected off the main axis: light from the Xe flash lamp scattered by the shocked sample and emission from the sample itself. Comparing the time dependence of this signal to the pure emission experiments, we were able to separate the scattering and emission components.

Time-resolved Raman spectroscopy measurements were performed as described previously.[6,40–42] The Raman spectroscopy system covered Stokes shifts from 800 to 3300 cm^{-1}. We were particularly interested in the CH stretching region from 2700 to 3300 cm^{-1}, because changes in these modes are indicative of the $\alpha-\gamma$ phase transition.[6,7,43] A single 514.5 nm laser pulse of 2 μs duration and 40 mJ energy excited the sample. The spectral resolution for Raman measurements was $\sim$20 cm^{-1} and time resolution was $\sim$40 ns.

III. Results and Discussion

Phase Transition Prior to Chemical Decomposition. In previous studies, we observed the $\alpha-\gamma$ phase transition in RDX single crystals shocked to peak stresses between 4.5 and 5.5 GPa,[6] and found no measurable dependence on crystal orientation. We also observed a phase transition time of about 100 ns at 5.5 GPa peak stress.

To determine whether the phase transition precedes initiation at higher stresses, a time-resolved Raman experiment was performed at 10 GPa. Selected time-dependent Raman spectra are shown in Figure 2. The spectrum at -155 ns is of unshocked RDX, i.e., before the shock wave entered the crystal. The next two spectra correspond to steps in the loading process. The spectrum at 590 ns was collected after the sample attained peak stress. A static pressure Raman spectrum at 9.8 GPa is shown for comparison.[7] Note the similarity between the spectral features in the static pressure results and the spectra acquired under shock loading. The spectrum at 345 ns also contains spectral features of the high pressure phase. This result indicates that the phase transition occurred quickly, as expected,[6] and that it was complete by the time peak stress was achieved.

Beginning at about 400 ns, broadband emission was detected. After 600 ns, Raman features could no longer be resolved because of this intense emission. A second Raman experiment at 16 GPa peak stress was attempted; however, the broadband emission overtook the Raman signal and saturated the detection system prior to attaining peak stress. Some shifting of the Raman peaks was observed, and it appeared that the phase transition had taken place, but the quality of the Raman data was poor. The results of this experiment made it clear that Raman measurements beyond 10 GPa are of limited value. However, these results show that the $\alpha-\gamma$ phase transition takes place before the initiation of chemical reactions.

Emission Spectroscopy. Emission spectroscopy experiments were performed with peak stresses ranging from 7 to 20 GPa. Figure 3 compares the spectrally integrated emission intensity for these different experiments as a function of time. (The 9.9 GPa experiment was performed with a different detection system than the others and is not included in this comparison. Also, the 9.8 and 9.9 GPa experiments used a slightly different optical arrangement that limited detection to 700 nm.) The shock wave enters the crystal at 0 ns. The data are cut off when release waves enter the RDX crystal because the sample is no longer under uniaxial strain; after this time emission intensity decreases. Note the significant increase in emission intensity between the 9.8 and 11.5 GPa experiments. For experiments with a peak stress between 7 and 13 GPa, there is a transition time of roughly 300−400 ns before the emission occurs. In the 20 GPa experiment, emission was observed during the first step in the loading process. Because of the window configuration in this experiment, the stress during the first step was significantly higher than in other experiments.[35] Figure 4 contains calculated

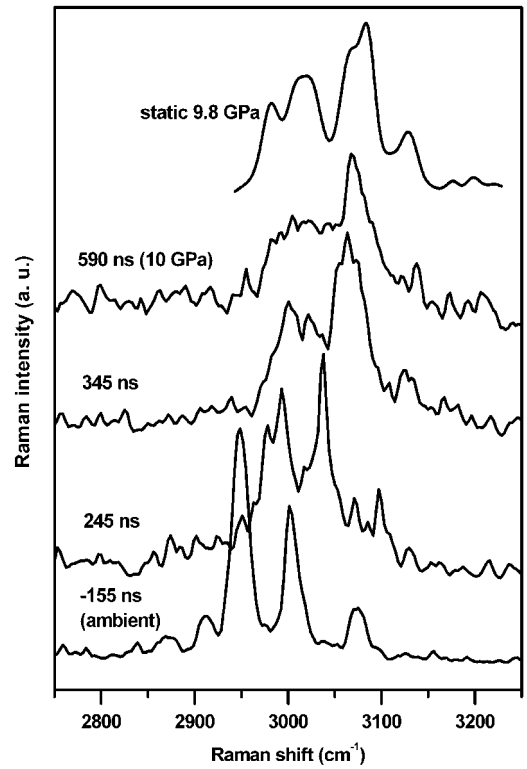

Figure 2. Time-dependent Raman spectra of the C−H stretching modes of [111] oriented RDX shocked to 10 GPa. Shock wave enters crystal at 0 ns. 95% of peak stress is reached at about 400 ns. After about 600 ns, Raman features can no longer be resolved from the broadband emission. Static pressure Raman spectrum at 9.8 GPa shown for comparison.[7] Spectra offset for clarity.

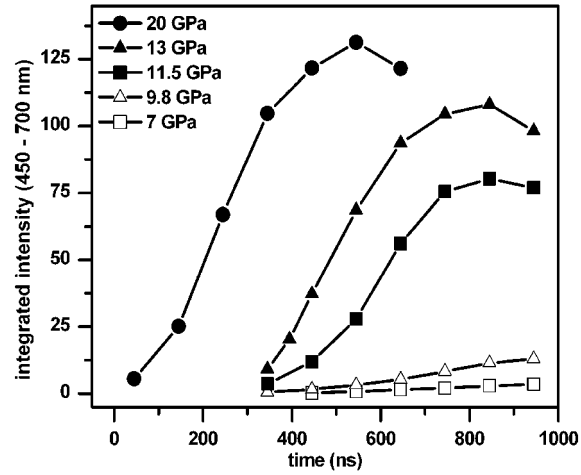

Figure 3. Spectrally integrated emission intensity plotted vs time for different peak stress experiments. Shock wave enters crystal at 0 ns.

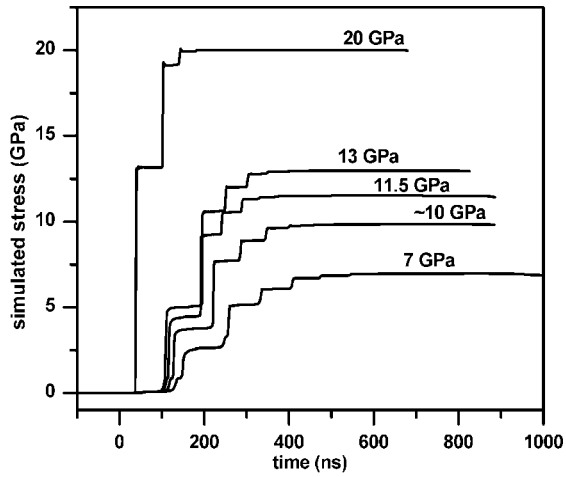

Figure 4. Simulated stress histories computed at the midpoint of the RDX crystal. Stress history is cutoff at the time at which release waves arrive. The shock wave enters the front of the crystal at 0 ns.

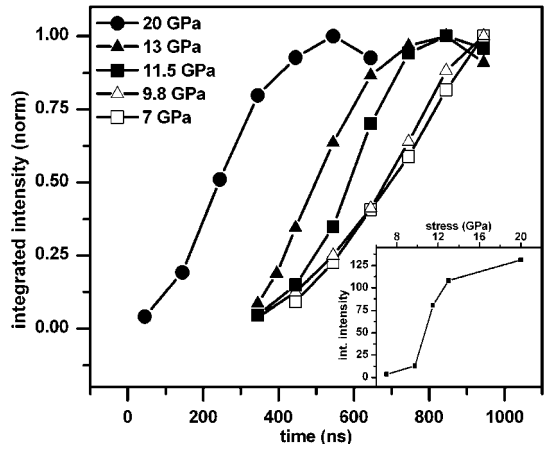

Figure 5. Normalized integrated intensity plots. Rise of emission occurs more rapidly as stress increases. Shock enters sample at 0 ns. Inset: spectrally integrated intensity as a function of peak stress at the time of maximum intensity.

stress histories for these experiments. Except in the 20 GPa experiment, emission does not begin until the sample has reached peak stress.

Figure 5 contains the same integrated intensity data after normalization to the peak value shown in Figure 3. This procedure allows the temporal profile of the emission from the lower stress experiments to be seen. Note the similarity between the 7 and 9.8 GPa traces. In the 11.5 and 13 GPa experiments, the emission intensity rises more quickly. There is also some decrease in the transition time for the 11.5 and 13 GPa experiments compared to the lower stress shots. The inset of Figure 5 shows the spectrally integrated intensity as a function of peak stress at the time of maximum intensity. The significant rise in intensity from 9.9 to 11.5 GPa is again clearly seen.

Spectral profiles from four experiments (7, 9.8, 13, and 20 GPa) are shown in Figures 6 and 7. All emission spectra have been corrected for the wavelength dependent response of the detection system.[3] In Figure 6, the chosen times correspond to an integrated emission of roughly 20% of the maximum intensity. The chosen times in Figure 7 correspond to the maximum emission intensity. Several features can be observed by comparing these spectra. For purposes of discussion, the emission spectrum will be divided into three regions. The first region represents wavelengths longer than 650 nm and is termed LW (long wavelength). The second is called VIS (visible) and includes wavelengths from 400 to 650 nm. The third component covers wavelengths shorter than 400 nm and is labeled UV. These designations will be used throughout the remainder of this paper.

For the early time spectra (Figure 6) in the 7, 9.8, and 13 GPa experiments, the UV and VIS components are significant. In the 20 GPa experiment, the LW component dominates the emission spectrum. In the later time spectra (Figure 7) at 13 and 20 GPa, the LW component tends to dominate the spectrum. However, the spectra from the 7 and 9.8 GPa experiments still contain a significant contribution from the VIS component. The 7 GPa spectrum also has a strong UV component.

These trends become clearer when we compare the relative intensities at 650 and 450 nm as a function of time for each experiment. These wavelengths are located near the boundaries of the VIS and UV spectral regions. This comparison, shown in Figure 8, gives a qualitative sense of the profile of the emission spectrum. For the two lowest stress experiments, 7 and 9.8 GPa, the profile of the emission spectrum did not change significantly with time. This is indicated by the flat response at a relative intensity of ~2. The emission spectrum from the 20 GPa experiment also does not change with time. However, it has a very different profile, with a relative intensity of ~8. The emission spectrum from the 9.9 GPa experiment starts out with a profile similar to that of the 7 GPa experiment but gradually comes to resemble the 20 GPa experiment. The same is true for the 11.5 and 13 GPa experiments; in each case, the emission spectrum initially resembles the 9.8 GPa spectrum then later appears more like the 20 GPa spectrum. It is also of note that the time required for the spectral change to occur decreases with increasing stress.

These results, together with the integrated emission traces in Figure 3 and Figure 5, indicate a threshold behavior between 9.8 and 11.5 GPa. Below 9.8 GPa, the emission spectrum contains all three spectral components and does not change significantly within the time window of the experiment (1000 ns). As peak stress rises, emission intensity increases and the spectral profile of the emission changes, with the LW component dominating the emission spectrum. The transition time for these spectral changes decreases as the stress increases. The difference between the 9.8 and 9.9 GPa experiments either is due to sample-to-sample variability or indicates a threshold very close to 10 GPa.

Source of Observed Emission. There are four possible sources of the observed emission: (i) thermal emission, (ii) electronically excited RDX molecules, (iii) mechanoluminescence from the crystal, or (iv) emission from excited decomposition intermediates. Each possible source will be discussed in turn.

To investigate the possibility of thermal emission, selected emission spectra were fit to a blackbody emission curve. The results of this fitting strongly suggest that the detected light is not due to thermal emission for several reasons. In the experiments at 9.9 and 13 GPa, the late time emission spectra were fit best with temperatures of 3000 and 2500 K, respectively. This is contrary to the expectation that temperature would increase with the stress. In addition, for spectra from different times in the 13 GPa experiment, the temperature determined from the fitting decreases as time increases. Again this is contrary to expectations.

Finally, these temperatures are significantly higher than expected for RDX in the very early stages of decomposition. Estimates of the temperature of unreacted, shocked RDX range

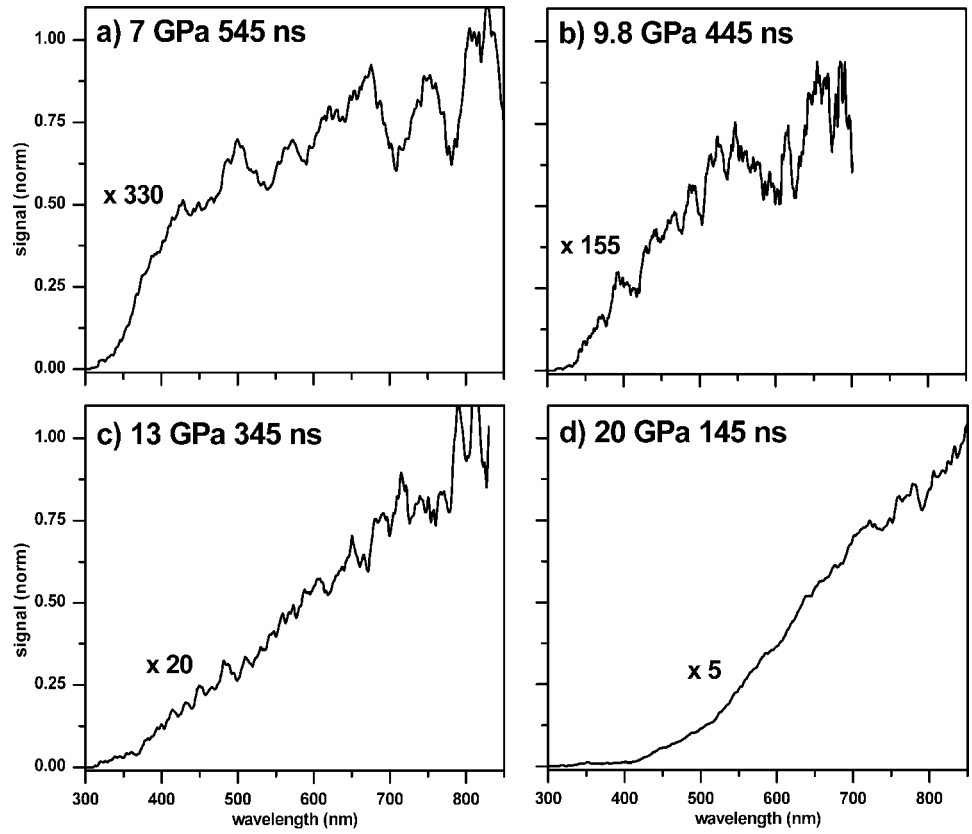

Figure 6. Early time emission spectra from four shock experiments: (a) 7, (b) 9.8, (c) 13 and (d) 20 GPa. Multiplication factors indicate relative intensity compared to the 20 GPa, 545 ns spectrum in Figure 7. Shock enters sample at 0 ns.

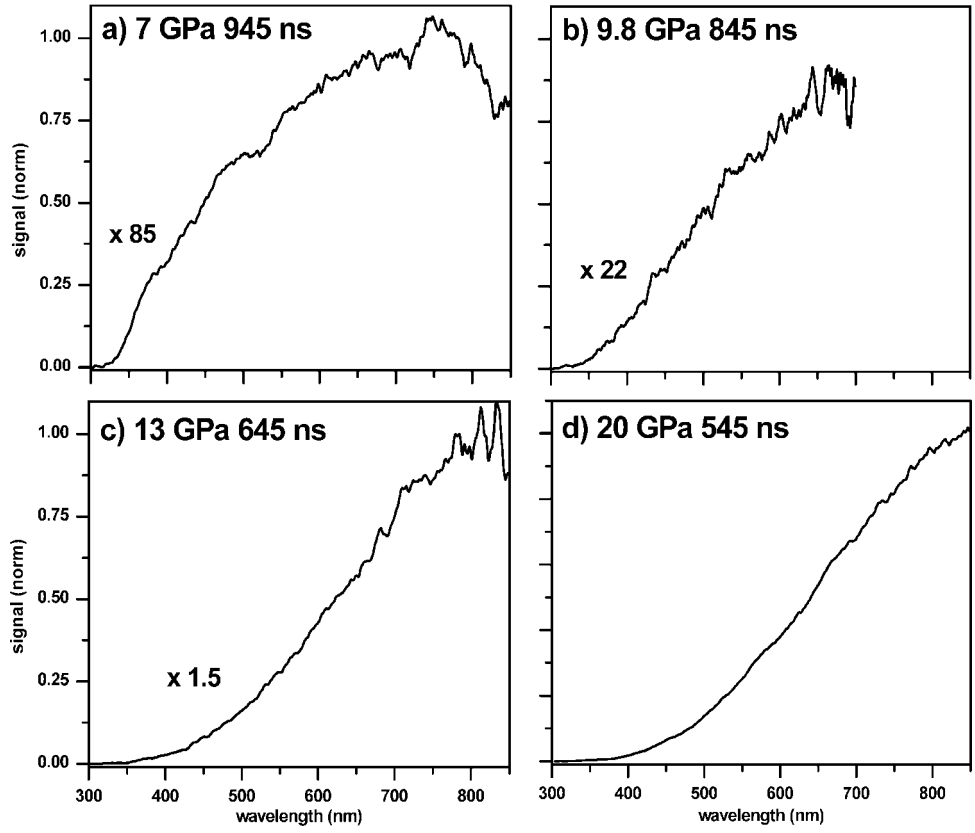

Figure 7. Late time emission spectra from the same four experiments depicted in Figure 5. Multiplication factors indicate relative intensity compared to the 20 GPa, 545 ns spectrum Shock enters sample at 0 ns. Peak stresses were (a) 7, (b) 9.8, (c) 13 and (d) 20 GPa.

from 500 to 750 K, depending on the loading path of the experiment.[35] The high temperatures indicated by the fitting could be reached in a fully developed detonation wave, but the small sample thickness (400 μm) prevents these conditions from

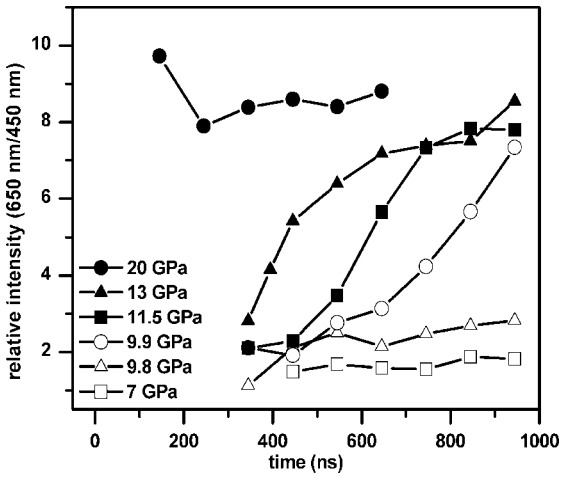

Figure 8. Time dependent relative intensities at 650 and 450 nm from six shock experiments. Experiments at 7 and 9.8 GPa show no significant time dependence in the emission spectrum. Experiments at 9.9, 11.5 and 13 GPa show a change in the emission spectrum. Onset of the change occurs earlier as the stress increases. The 20 GPa emission spectrum does not change with time. Shock enters sample at 0 ns.

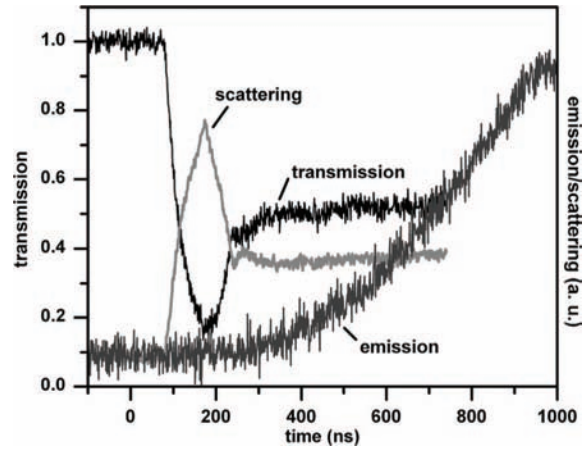

Figure 9. Time dependent emission, transmission and scattering photodiode records from two experiments at 9.9 GPa. Shock enters sample at 0 ns.

being reached in our experiments. Void collapse or formation of shear bands could lead to localized high temperatures; however, we would expect the temperature to increase with stress and time, contrary to the results of our fitting analysis. On the basis of all these considerations, the observed emission is not attributed to thermal radiation.

We do not believe that emission from excited states of RDX is a contributing factor for the following reasons. First, there is little evidence that the excited states of RDX are luminescent. One paper reported fluorescence from RDX powder,[44] but other investigators have reported no fluorescence from RDX.[45] Attempts in our laboratory to observe fluorescence from RDX single crystals and powder were unsuccessful. For this reason, no attempts were made to measure fluorescence of RDX under high pressure. If RDX does fluoresce, the process is apparently inefficient. Second, the reported RDX fluorescence is peaked in the visible region, around 550 nm. Our observed emission spectrum does not at all match the published fluorescence spectrum.[44] (The possibility of luminescence from the thin layer of glycerol was explored previously and found not to be a concern.[3])

Fractoluminescence, pyroelectric luminescence, or some other mechanoluminescence phenomenon seems unlikely on the basis of symmetry and other considerations. It is generally required that a crystal be piezoelectric to exhibit mechanoluminescence.[46] However, both the α and γ phases of RDX are of D_{2h} crystal symmetry and are nonpiezoelectric.[7] It has also been stated that mechanoluminescence spectra often resemble the photoluminescence spectrum of the material[46,47] but, as discussed previously, the observed emission does not match the reported fluorescence of RDX.

The temporal behavior of the emission also argues against it being from either excited RDX or mechanoluminescence. If RDX molecules are produced in excited electronic states, they should be excited as the shock wave passes through the material and begin to luminesce promptly thereafter. However, we observed the emission to have a transition time of a few hundred nanoseconds and to increase in intensity after peak stress is achieved. The same argument can be applied to the mechanoluminescence hypothesis. Such emission should occur as the material is deformed, which will happen during the stepwise loading, and not be delayed until after the final stress state has been reached.

On the basis of the above considerations, we attribute the observed emission to luminescence from species produced during RDX decomposition. Identifying these products is crucial for developing a decomposition mechanism for shocked RDX. Unlike PETN,[3] the emission spectrum of shocked RDX is generally featureless. Despite this limitation, there are features that can be used to discern the underlying chemical mechanisms. One key is the dominance of the LW component, particularly at higher stress and later in time when the extent of reaction should be greatest. The source of this LW emission is likely an intermediate in the decomposition of RDX. Variation in the relative intensity of portions of the emission spectrum also gives us indications to the underlying chemical reactions. This change in the emission spectrum suggests a change in the concentrations of the emitting species and possibly a change in the chemical mechanism. Before discussing chemical mechanisms further, we need to account for all the light produced during decomposition.

Complementary Transmission/Scattering Experiments. In the work on PETN single crystals we learned how to correct emission spectra for reabsorption within the sample.[3] Therefore, transmission experiments were performed on RDX to measure the time-dependent extinction spectrum. In the case of PETN, scattering from the shocked crystal was determined to be negligible and all extinction was attributed to absorption within the sample. To examine this issue in RDX, we added detectors off the main optic axis to measure light that was scattered from the sample during the shock experiment.

Figure 9 contains time dependent transmission, scattering and emission records from the two experiments at 9.9 GPa. The shock wave enters the crystal at 0 ns, and the transmission decreases significantly soon thereafter. This drop in transmission is accompanied by a corresponding increase in scattering. The temporal response of scattered light shows a peak and then decreases and finally levels off. The temporal response of the scattered light correlates well with the transmission trace, suggesting that a significant portion of the transmission loss is due to scattering phenomena. After the leveling off of the transmission/scattering signal, the emission signal begins to appear. This temporal separation between the two traces suggests that the underlying phenomena are not directly connected. The extinction/scattering is likely due to a macroscopic response of the crystal to shock loading, such as cracking or plastic deformation.[48] Because of the strong scattering signal, we cannot

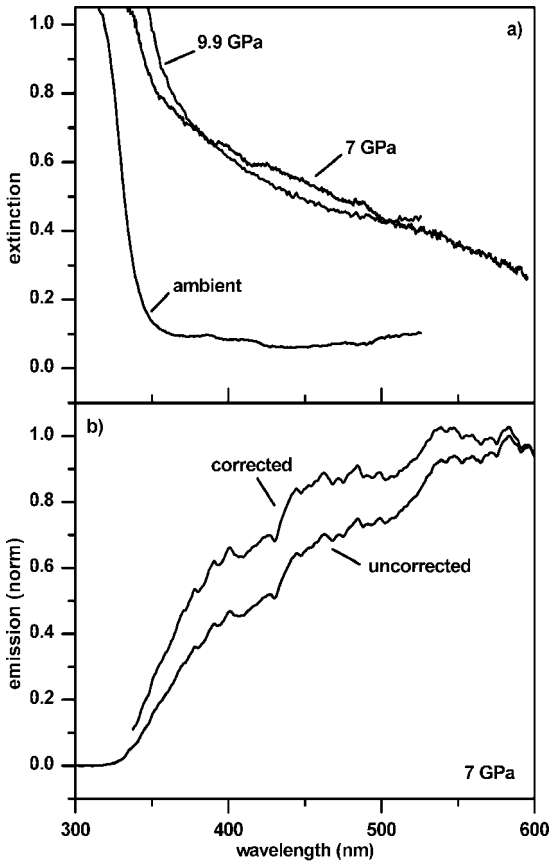

Figure 10. (a) Extinction spectra at ambient, 7 and 9.9 GPa. Note the overall similarity between the 7 and 9.9 GPa extinction spectra. At wavelengths longer than ~375 nm, the majority of extinction is due to scattering. Dynamic range of detection system limits maximum extinction. (b) Uncorrected and corrected emission spectra from 7 GPa experiment. Correction based on assumptions made in PETN work (ref 3).

completely separate the scattering and absorption components of the extinction as was possible for PETN.[3]

Figure 10a compares the extinction spectra of the 7 and 9.9 GPa transmission experiments. An ambient absorption spectrum is included for comparison. The dynamic range of the detection system limits the extinction that can be measured to about 1.1. When RDX is shocked, the absorption edge shifts somewhat, but there is a long tail in the extinction spectrum that we attribute primarily to scattering. The extinction spectrum was not observed to change in time, unlike the 9.9 GPa emission spectrum. This suggests that the changes in the emission spectrum are not due to time dependent extinction phenomena. The 13 GPa transmission experiment produced limited results because the extinction levels exceeded the dynamic range of 1.1 over the entire spectral range. The scattering signal was also strong, again suggesting that the majority of the extinction is due to scattering and not absorption.

The technique used to correct the emission spectra for absorption in the PETN work[3] was also used to correct RDX emission for extinction. This procedure assumes that all extinction is due to absorption and that the distribution of the emitting and absorbing species is uniform throughout the thickness of the sample. The corrected emission spectrum for the 7 GPa experiment is shown in Figure 10b. The results of this correction suggest that some additional light in the UV and VIS components may exist and our interpretation of the results should keep this in mind. However, the observation of significant scattering by shocked RDX violates the first assumption. The second assumption is reasonable, but the correction procedure seems to be of limited value for RDX. Thus, the uncorrected spectra were used in the discussion of the emission results.

The results of the transmission/scattering experiments suggest that the RDX crystal becomes "opaque" under shock wave loading and that the emission is produced primarily from a thin layer of material at the back of the sample. Inelastic deformation and/or the $\alpha-\gamma$ phase transition likely cause the scattering. The extinction does not appear to be a molecular-level phenomenon, except for wavelengths shorter than about 350 nm. Because we were unable to determine the exact source of the scattering or the size of the scattering centers, we cannot assign a wavelength dependence to the scattering. Therefore, the uncorrected emission spectra form the basis of our development of a decomposition mechanism, with the understanding that what we have observed represents a lower limit to the light produced during decomposition, particularly for the VIS and UV components.

General Features of RDX Decomposition Mechanism. Though a complete understanding of shock induced decomposition cannot be developed solely from the experimental results, several important observations can be made. First, the results of the 10 GPa peak stress Raman experiment clearly indicate that the $\alpha-\gamma$ phase transition takes place at this stress prior to the onset of decomposition. Because of comparable transition times for the $\alpha-\gamma$ phase transition and emission, we believe that decomposition begins from the γ phase.

We observed a broad emission spectrum from 350−850 nm. On the basis of the observed spectral changes, we noted three characteristic regions in this spectrum. In principle, these three regions could be produced by three different chemical species. The early decomposition reactions produce all three emission components, whereas the emission at higher stress and later in time is dominated by the LW emission component. We use the features of the emission spectra to gain insight into the decomposition chemistry of RDX. It should be noted that a fully developed detonation wave is never formed in our studies. The run distance to detonation for RDX is several mm,[49] whereas our samples are only 400 μm thick. Therefore, we focus on simple chemical reactions that are plausible during the earliest stages of decomposition.

The decomposition chemistry of RDX and other nitramine high explosives is governed largely by the nitro functional groups. The NO_2 radical likely plays an important role in RDX decomposition. The luminescence spectrum of excited NO_2 is very broad, almost forming a continuum.[50–52] The peak of this continuum emission varies depending on the conditions under which the excited NO_2 was produced, and can vary from the visible (500−600 nm)[52–56] to the near-infrared (1200 nm).[50,51,54,57,58] Because of the differences in the experimental conditions, our results are not directly comparable to these other studies. Temperature and pressure effects likely change the emission spectrum of NO_2. However, these studies show that NO_2 emission can vary greatly over a wide spectral range and suggest that NO_2 is a plausible source of the observed LW emission.

Comparing our experimental results with those reported in the literature for various fragments of RDX, we tentatively assign the LW component to the emission of NO_2. NO_2 can be a direct product of N−N homolysis and probably plays an important role in the shock wave induced decomposition of RDX. Additional support for this assignment is presented in our companion paper.[1]

We now need to assign the other components of the emission spectrum to other species. NO_2 exhibits a dissociation limit in the emission spectrum at about 390 nm.[50] This suggests that

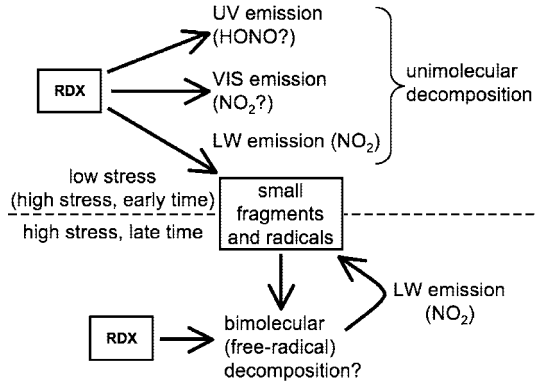

Figure 11. Outline of RDX decomposition. Initial unimolecular decomposition leads to products that generate three emission components. A dashed line indicates the stress threshold in the decomposition mechanism. Above the 10 GPa threshold, bimolecular reactions between radicals and RDX begin a second decomposition cycle. This pathway leads to production of NO_2 and the LW component dominates the emission spectrum.

the source of the UV component is not NO_2. One possible source is HONO, which can also be produced early in the decomposition of RDX[14] and can emit in the range 315−385 nm.[59] Another possible source of UV emission is NO, which can produce emission over the range 200−650 nm.[60] NO has been observed in the photodecomposition of RDX[34] and as a decomposition product in molecular dynamics simulations.[61] However, we have not been able to identify a simple mechanism to produce NO under the conditions of our experiments.[1] Thus we favor HONO as the source of the UV emission. As discussed earlier, it is possible that even more light is produced in the UV spectral region than was observed and our mechanism must consider that possibility.

The final portion of the emission spectrum that must be assigned is the VIS component. Emission from NO_2 has been observed in this region. For example, photolysis of RDX by UV laser light leads to significant emission between 450 and 650 nm.[56] This method of producing excited NO_2 is different from our shock wave experiments, but this result suggests that the VIS component could also be due to NO_2. As discussed further in our companion paper,[1] the rich electronic structure of NO_2 can account for all these observations. We must also consider other possible species as the source of the VIS component. Sources of the UV and VIS components are proposed and discussed further in the companion paper.[1]

Solely on the basis of the experimental results, we can summarize the decomposition of shocked RDX as follows. Initially, the RDX single crystal undergoes a transition to the high pressure γ phase at approximately 4.5 GPa and within a few hundred nanoseconds. Significant scattering indicates micro- and macroscopic level changes within the crystal due to inelastic deformation and/or the phase transition.

Within 100 ns after reaching peak stress, decomposition begins and light is emitted. The decomposition process is depicted schematically in Figure 11. The first stage of decomposition leads to the production of multiple emitting species, including NO_2, as indicated by the broad emission spectrum that begins at about 350 nm and extends into the near-infrared. For peak stress above 10 GPa, a subsequent decomposition channel opens that leads to greater production of NO_2 radicals. This reaction channel also leads to accelerated decomposition, as indicated by the significant rise in integrated intensity. One possibility for this acceleration stage is the onset of bimolecular reactions between free-radicals and unreacted RDX molecules. This mechanism can perpetuate the cycle with accelerated formation of NO_2 that contributes to the LW emission spectrum. Details of the decomposition mechanism require the identification of chemical reactions through quantum chemical calculations. These calculations, presented in the companion paper,[1] provide further insight into sources of emitting species and decomposition mechanism consistent with the experimental results.

IV. Concluding Remarks

Real time, optical spectroscopy measurements were obtained to improve our understanding of the shock-induced decomposition of RDX. Time-resolved emission spectroscopy was particularly useful toward this end. We observed a threshold in the response of RDX at a shock stress of about 10 GPa for [111] oriented crystals. At low stresses, the emission spectrum is broad (350−850 nm) and the spectral profile does not change temporally. Above this stress, the extent of reaction (as determined by the emission output) increased considerably. We also observed temporal changes in the emission spectrum above this threshold. For experiments above the 10 GPa threshold, the emission spectrum initially resembled that of the low stress experiments but changed with the long wavelength portion of the spectrum displaying stronger intensity. The onset time for this change decreased as peak stress increased.

On the basis of the experimental results, we propose that NO_2 is an important species in the initial decomposition of RDX, supported by the broad emission spectrum with a strong long wavelength component. This assignment is also supported by quantum chemistry calculations on RDX molecules and likely decomposition intermediates, as discussed in our companion paper.[1] Other species are involved in the initial steps of the decomposition, but we cannot definitively identify them from the experimental data alone. HONO and NO are possible species. We also propose that the decomposition mechanism changes at stresses above the 10 GPa threshold. This change likely involves bimolecular reactions between RDX and radical decomposition products. In the companion paper,[1] we build on the experimental results and utilize quantum chemical calculations to develop a comprehensive decomposition mechanism.

Acknowledgment. We thank Dr. Daniel E. Hooks of the Los Alamos National Laboratory for providing the RDX crystals. Dr. J. Michael Winey is thanked for the stress wave and temperature calculations. Kurt Zimmerman and Kent Perkins are thanked for their assistance in performing the shock experiments. This work was supported by ONR MURI Grants N00014-01-1-0802 and N00014-06-1-0459, and DOE Grant DEFG0397SF21388.

References and Notes

(1) Miao, M.; Dreger, Z. A.; Patterson, J. E.; Gupta, Y. M. *J. Phys. Chem. B* **2008**, *112*, 7383.
(2) Gruzdkov, Y. A.; Gupta, Y. M. *J. Phys. Chem. A* **2000**, *104*, 11169.
(3) Dreger, Z. A.; Gruzdkov, Y. A.; Gupta, Y. M.; Dick, J. J. *J. Phys. Chem. B* **2002**, *106*, 247.
(4) Gruzdkov, Y. A.; Dreger, Z. A.; Gupta, Y. M. *J. Phys. Chem. A* **2004**, *108*, 6216.
(5) Hemmi, N.; Dreger, Z. A.; Gruzdkov, Y. A.; Winey, J. M.; Gupta, Y. M. *J. Phys. Chem. B* **2006**, *110*, 20948.
(6) Patterson, J. E.; Dreger, Z. A.; Gupta, Y. M. *J. Phys. Chem. B* **2007**, *111*, 10897.
(7) Dreger, Z. A.; Gupta, Y. M. *J. Phys. Chem. B* **2007**, *111*, 3893.
(8) Owens, F. J.; Sharma, J. *J. Appl. Phys.* **1980**, *51*, 1494.
(9) Forbes, J. W.; Tasker, D. G.; Granholm, R. H.; Gustavson, P. K. In *Shock Compression of Condensed Matter* - 1989 Schmidt, S. C., Johnson, J. N., Davison, L. W., Eds.; AIP: New York; *1990*; p 709.

(10) Delpuech, A.; Cherville, J.; Michaud, C. In *Proc. Seventh Symp. (Int.) on Detonation*; Short, J. M., Ed.; Naval Surface Weapon Center, US Naval Academy: Annapolis, MD, 1981; p 36.
(11) Delpuech, A.; Mentil, A.; Pouligny, B. In *Shock Waves Condens. Matter - 1985*; Gupta, Y. M., Ed.; Plenum: New York; 1986; p 877.
(12) Sandusky, H. W.; Beard, B. C.; Glancy, B. C.; Elban, W. L.; Armstrong, R. W. *Mater. Res. Soc. Symp. Proc.* **1993**, *296*, 93.
(13) Van der Meer, B. J. In *Chemistry and Physics of Energetic Materials*; Bulusu, S. N., Ed.; Kluwer Academic Publishers: 1990; Vol. 309, pp 653.
(14) Chakraborty, D.; Muller, R. P.; Dasgupta, S.; Goddard, W. A., III *J. Phys. Chem. A* **2000**, *104*, 2261.
(15) Zhao, X.; Hintsa, E. J.; Lee, Y. T. *J. Chem. Phys.* **1988**, *88*, 801.
(16) Farber, M. *Mass Spec. Rev.* **1992**, *11*, 137.
(17) Habibollahzadeh, D.; Grodzicki, M.; Seminario, J. M.; Politzer, P. *J. Phys. Chem.* **1991**, *95*, 7699.
(18) Botcher, T. R.; Wight, C. A. *J. Phys. Chem.* **1994**, *98*, 5441.
(19) Wu, C. J.; Fried, L. E. *J. Phys. Chem. A* **1997**, *101*, 8675.
(20) Wight, C. A.; Botcher, T. R. *J. Am. Chem. Soc.* **1992**, *114*, 8303.
(21) Melius, C. F. In *Chemistry and Physics of Energetic Materials*; Bulusu, S. N., Ed.; Kluwer Academic Publishers: Dordrecht, The Netherlands, 1990; Vol. 309; pp 21.
(22) Adams, G. F.; Shaw, R. W. *Annu. Rev. Phys. Chem.* **1992**, *43*, 311.
(23) Harris, N. J.; Lammertsma, K. *J. Am. Chem. Soc.* **1997**, *119*, 6583.
(24) Pace, M. D.; Moniz, W. B. *J. Magn. Reson.* **1969**, *1982* (47), 510.
(25) Owens, F. J. *THEOCHEM* **1996**, *370*, 11.
(26) Swadley, M. J.; Li, T. *J. Chem. Theory Comput.* **2007**, *3*, 505.
(27) Naud, D. L.; Brower, K. R. *J. Org. Chem.* **1992**, *57*, 3303.
(28) Wang, J.; Brower, K. R.; Naud, D. L. *J. Org. Chem.* **1997**, *62*, 9055.
(29) Behrens, R.; Bulusu, S. *J. Phys. Chem.* **1991**, *95*, 5838.
(30) Behrens, R.; Bulusu, S. *J. Phys. Chem.* **1992**, *96*, 8877.
(31) Behrens, R., Jr.; Bulusu, S. *J. Phys. Chem.* **1992**, *96*, 8891.
(32) Behrens, R. *J. Phys. Chem.* **1990**, *94*, 6706.
(33) Bulusu, S.; Weinstein, D. I.; Autera, J. R.; Velicky, R. W. *J. Phys. Chem.* **1986**, *90*, 4121.
(34) Greenfield, M.; Guo, Y. Q.; Bernstein, E. R. *Chem. Phys. Lett.* **2006**, *430*, 277.
(35) Winey, J. M. Personal communication.
(36) Gupta, Y. M. *COPS code*; Stanford Research Institute: Menlo Park, CA, 1976, unpublished.
(37) Winey, J. M.; Gupta, Y. M. *J. Phys. Chem. A* **1997**, *101*, 9333.
(38) Gruzdkov, Y. A.; Gupta, Y. M. *J. Phys. Chem. A* **1998**, *102*, 2322.
(39) Constantinou, C. P.; Winey, J. M.; Gupta, Y. M. *J. Phys. Chem.* **1994**, *98*, 7767.
(40) Yoo, C. S.; Gupta, Y. M.; Horn, P. D. *Chem. Phys. Lett.* **1989**, *159*, 178.
(41) Gustavsen, R. L.; Gupta, Y. M. *J. Appl. Phys.* **1994**, *75*, 2837.
(42) Pangilinan, G. I.; Gupta, Y. M. *J. Phys. Chem.* **1994**, *98*, 4522.
(43) Baer, B. J.; Oxley, J.; Nicol, M. *High Press. Res.* **1990**, *2*, 99.
(44) Marinkas, P. L. *J. Lumin.* **1977**, *15*, 57.
(45) Stals, J.; Barraclough, C. G.; Buchanan, A. S. *Trans. Faraday Soc.* **1969**, *65*, 904.
(46) Chandra, B. P. *Mechanoluminescence. In Luminescence of Solids*; Vij, D. R., Ed.; Plenum Press: New York, 1998; pp 361.
(47) Kalinowski, J.; Dreger, Z. A. *Phys. Rev. B* **1987**, *36*, 7840.
(48) Hooks, D. E.; Ramos, K. J.; Martinez, A. R. *J. Appl. Phys.* **2006**, *100*, 024908.
(49) Massoni, J.; Saurel, R.; Baudin, G.; Demol, G. *Phys. of Fluids* **1999**, *11*, 710. This paper describes HMX; however, RDX exhibits a similar run distance to detonation.
(50) Levitt, B. P. *J. Chem. Phys.* **1965**, *42*, 1038.
(51) Braun, W.; Kurylo, M. J.; Kaldor, A.; Wayne, R. P. *J. Chem. Phys.* **1974**, *61*, 461.
(52) Inoue, G.; Nakata, Y.; Usui, Y.; Akimoto, H.; Okuda, M. *J. Chem. Phys.* **1979**, *70*, 3689.
(53) Fontijn, A.; Meyer, C. B.; Schiff, H. I. *J. Chem. Phys.* **1964**, *40*, 64.
(54) Paulsen, D. E.; Sheridan, W. F.; Huffman, R. E. *J. Chem. Phys.* **1970**, *53*, 647.
(55) Butler, L. J.; Krajnovich, D.; Lee, Y. T.; Ondrey, G.; Bersohn, R. *J. Chem. Phys.* **1983**, *79*, 1708.
(56) Capellos, C.; Papagiannakopoulos, P.; Liang, Y. L. *Chem. Phys. Lett.* **1989**, *164*, 533.
(57) Clyne, M. A. A.; Thrush, B. A.; Wayne, R. P. *Trans. Faraday Soc.* **1964**, *60*, 359.
(58) Schurath, U.; Lippmann, H. H.; Jesser, B. *Ber. Bunsen-Ges.* **1981**, *85*, 807.
(59) Herzberg, G. *Molecular Spectra and Molecular Structure III. Electronic Spectra and Electronic Structure of Polyatomic Molecules*; van Nostrand Reinhold: New York, 1966; p 614.
(60) Suchard, S. N. *Spectroscopic Data, Vol. 1 Heteronuclear Diatomic Molecules*; IFI/Plenum: New York, 1975; p 720.
(61) Strachan, A.; van Duin, A. C. T.; Chakraborty, D.; Dasgupta, S.; Goddard, W. A. *Phys. Rev. Lett.* **2003**, *91*, 098301/1.

JP800827B